

# 1 Path-integral method for the source apportionment of 2 photochemical pollutants

3  
4 **A. M. Dunker<sup>1</sup>**

5 [1]{A. M. Dunker, LLC, Bloomfield Hills, Michigan, USA}

6 Correspondence to: A. M. Dunker (amdunker@gmail.com)

## 7 8 **Abstract**

9 A new, path-integral method is presented for apportioning the concentrations of pollutants  
10 predicted by a photochemical model to emissions from different sources. A novel feature of  
11 the method is that it can apportion the difference in a species concentration between two  
12 simulations. For example, the anthropogenic ozone increment, which is the difference between  
13 a simulation with all emissions present and another simulation with only the background (e.g.,  
14 biogenic) emissions included, can be allocated to the anthropogenic emission sources. The  
15 method is based on an existing, exact mathematical equation. This equation is applied to relate  
16 the concentration difference between simulations to line or path integrals of first-order  
17 sensitivity coefficients. The sensitivities describe the effects of changing the emissions and are  
18 accurately calculated by the decoupled direct method. The path represents a continuous  
19 variation of emissions between the two simulations, and each path can be viewed as a separate  
20 emission-control strategy. The method does not require auxiliary assumptions, e.g., whether  
21 ozone formation is limited by the availability of volatile organic compounds (VOC's) or  
22 nitrogen oxides (NO<sub>x</sub>), and can be used for all the species predicted by the model. A simplified  
23 configuration of the Comprehensive Air Quality Model with Extensions is used to evaluate the  
24 accuracy of different numerical integration procedures and the dependence of the source  
25 contributions on the path. A Gauss-Legendre formula using 3 or 4 points along the path gives  
26 good accuracy for apportioning the anthropogenic increments of ozone, nitrogen dioxide,  
27 formaldehyde, and nitric acid. Source contributions to these increments were obtained for paths  
28 representing proportional control of all anthropogenic emissions together, control of NO<sub>x</sub>  
29 emissions before VOC emissions, and control of VOC emissions before NO<sub>x</sub> emissions. There

1 are similarities in the source contributions from the three paths but also differences due to the  
2 different chemical regimes resulting from the emission-control strategies.

3

## 4 **1 Introduction**

5 The goal of source apportionment is to determine, quantitatively, how much different emission  
6 sources contribute to a given pollutant concentration. Source apportionment is thus a useful  
7 tool in developing efficient strategies to meet air quality standards by identifying the most  
8 important sources. If emissions are involved in only linear processes between where they are  
9 emitted and where they impact a receptor location, the concentration of the pollutant at the  
10 receptor is the sum of independent contributions from the individual emission sources. For  
11 example, one can define a tracer for each source of primary, unreactive particulate matter (PM)  
12 in an air quality model such that the sum of the tracer concentrations is the total primary PM  
13 concentration and the tracer concentrations form the source apportionment. However, if a  
14 secondary pollutant is formed by nonlinear chemical reactions, source apportionment is more  
15 complicated and, indeed, there is no unique apportionment.

16 Reflecting this non-uniqueness, a number of approaches have been developed for source  
17 apportionment of secondary pollutants. The simplest approach is source removal or the brute  
18 force method. Simulations with and without a particular source are compared, and the changes  
19 in predicted concentrations are assigned to emissions from that source (Marmur et al., 2006;  
20 Tong and Mauzerall, 2008; Wang et al., 2009; Zhang et al., 2014). A related approach is the  
21 factor-separation method, which for  $M$  sources involves analysis of a set of  $2^M$  simulations  
22 (Stein and Alpert, 1993; Tao et al., 2005). Each simulation includes emissions from a different  
23 source or a different combination of sources. Pollutant concentrations are assigned not just to  
24 sources but to interactions among sources.

25 Another approach involves the use of reactive tracers for individual chemical species, sources,  
26 and/or geographic regions (Yarwood et al., 1996; Dunker et al., 2002b; Mysliwiec and  
27 Kleeman, 2002; Wagstrom et al., 2008; Wang et al., 2009; Grewe et al., 2010; Butler et al.,  
28 2011; Emmons et al., 2012; Kwok et al., 2013). However, various chemical assumptions  
29 (beyond those in the chemical mechanism) are usually applied to track production of the  
30 secondary pollutant in nonlinear reactions. In addition, the source contributions are often  
31 restricted to be positive even if some primary pollutants can inhibit formation of the secondary  
32 pollutant. An exception is possible if tracers are assigned to all the chemical species and the

1 model has an appropriate form (Grewe, 2013). Then, chemical assumptions external to the  
2 model are unnecessary, and the source contributions need not be positive.

3 Assignment methods trace through all the reaction pathways from products back to parent  
4 reactants (Bowman and Seinfeld, 1994; Bowman, 2005). These methods also require extra  
5 chemical assumptions for reactions in which a product results from multiple reactants. Lastly,  
6 local sensitivity coefficients have been used to apportion ozone (O<sub>3</sub>) and PM (Dunker et al.  
7 2002b; Cohan et al., 2005; Koo et al., 2009). This approach involves constructing a Taylor  
8 series representation of the concentration as a function of source emissions and extrapolating  
9 the representation to zero emissions.

10 This work presents a new approach for source apportionment called the Path-Integral Method  
11 (PIM). The PIM provides a new, direct mathematical connection between sensitivity analysis  
12 and source apportionment and a connection between source apportionment and emission-  
13 control strategies. Also, the PIM does not require additional chemical assumptions beyond  
14 those in the model itself. An important advantage of the PIM is its ability to allocate to sources  
15 a concentration increment, i.e., the difference between two simulations (base and background  
16 cases). If the anthropogenic increment is allocated to sources, the PIM requires that the base-  
17 case concentration minus the sum of the anthropogenic source contributions equals the  
18 background concentration. Other methods do not have this requirement, and thus may ascribe  
19 too much or too little importance to the anthropogenic sources. The PIM does require more  
20 computational effort than some other source apportionment methods because first-order  
21 sensitivities must be calculated at several levels of anthropogenic emissions.

22 The PIM is applied here to allocate the anthropogenic increments of O<sub>3</sub> and other species using  
23 a 2-cell configuration of the Comprehensive Air Quality Model with Extensions (CAMx)  
24 (ENVIRON, 2013). Another application of the PIM using a detailed, 3-D CAMx configuration  
25 for the eastern U.S. will be reported elsewhere (Dunker et al., 2015).

26

## 27 **2 Description of the PIM**

### 28 **2.1 Equations**

29 The PIM is based on an exact mathematical equation that is in itself not new. In particular, the  
30 equation is routinely used in thermodynamics (Sect. 2.3). However, the application of the

1 equation to atmospheric modeling is new. The equation is the generalization to multiple  
 2 variables of a familiar relationship for a single variable, namely that the integral of the  
 3 derivative of a function ( $\int_a^b (df/dx) dx$ ) is equal to the difference in the value of the function  
 4 at the ends of the integration interval ( $f(b) - f(a)$ ).

5 For this work, the equation (Kaplan, 1959) takes the form

$$7 \quad \Delta c_i(\mathbf{x}, t) = c_i^1(\mathbf{x}, t; \mathbf{\Lambda} = 1) - c_i^0(\mathbf{x}, t; \mathbf{\Lambda} = 0) = \sum_{m=1}^M \int_P \frac{\partial c_i(\mathbf{x}, t; \mathbf{\Lambda})}{\partial \lambda_m} d\lambda_m$$

6 (1)

8 The  $c_i^1$  is the concentration of species  $i$  in the base case, with all emissions present, and  $c_i^0$  is  
 9 the concentration in the background case, with  $M$  emission sources removed.  $\mathbf{\Lambda}$  is the array of  
 10 the parameters  $\lambda_m$  that scale the emissions of the  $M$  sources. If all  $\lambda_m = 0$  ( $\mathbf{\Lambda} = 0$ ), the emissions  
 11 are those of the background case, and if all  $\lambda_m = 1$  ( $\mathbf{\Lambda} = 1$ ), the emissions are those of the base  
 12 case. The  $\partial c_i / \partial \lambda_m$  are the first-order sensitivities of  $c_i$  with respect to the scaling parameters.  
 13 The integrals on the right side of Eq. (1) are taken over a curve or path  $P$  in  $M$ -dimensional  
 14 space leading from the emissions in the background case to those in the base case. The  $\Delta c_i$  is  
 15 the difference between the concentrations in the base and background cases at the same spatial  
 16 location  $\mathbf{x}$  and time  $t$ .

17 Although the focus here is on emissions, Eq. (1) can also include parameters that scale the initial  
 18 and boundary concentrations. Furthermore, if the background case has all emissions and initial  
 19 and boundary concentrations set to zero, then  $c_i^0 = 0$  and  $\Delta c_i$  is the total concentration. Thus,  
 20 the PIM can allocate the total concentration in a simulation as well as concentration differences  
 21 between simulations.

22 The contribution of source  $m$  to  $\Delta c_i$ ,  $S_{im}$ , is defined to be

$$24 \quad S_{im}(\mathbf{x}, t; P) = \int_P \frac{\partial c_i(\mathbf{x}, t; \mathbf{\Lambda})}{\partial \lambda_m} d\lambda_m$$

23 (2)

25 The PIM does not strictly require that the source contributions be calculated for all  $M$  sources  
 26 or that  $\Delta c_i$  be calculated. The sensitivities can be determined for a subset of the sources and  
 27 integrated to obtain the  $S_{im}$  only for the sources of interest. However, if all the source  
 28 contributions and  $\Delta c_i$  are calculated, then Eq. (1) can be used to check the accuracy of the

1 integration procedure. The integration procedure can be modified then, if necessary, so that the  
 2 sum of the source contributions equals  $\Delta c_i$  within the desired error tolerance.

3 The source contributions depend on the path  $P$  from the point  $\Lambda = 0$  to the point  $\Lambda = 1$ . Because  
 4 there are an infinite number of paths between these two points, there are an infinite number of  
 5 sets of source contributions, one set corresponding to each path. Viewed in the direction of  
 6 integration, from  $\Lambda = 0$  to  $\Lambda = 1$ , emissions are added into the background case until the base  
 7 case is reached. Viewed in the opposite direction, emissions are controlled from the base case  
 8 until the background case is reached. Thus, each path  $P$  represents a possible emission-control  
 9 scenario, and the contribution of a given source to the change in concentration  $\Delta c_i$  depends on  
 10 the control scenario.

11 Because the sensitivities are integrated over the path  $P$  in Eq. (2), the PIM considers a range of  
 12 chemical conditions in calculating the source contributions, from zero to the full anthropogenic  
 13 emissions in the base case. Methods based on tracers or a Taylor series expansion (e.g., with  
 14 first- and second-order sensitivities) use only the emissions and the chemical conditions of the  
 15 base case. Thus, the PIM provides source contributions that are averaged over the emission-  
 16 control scenario, not specific to the base case.

17 The path  $P$  can be described via a path variable  $u$  that describes position along the path. Each  
 18  $\lambda_m$  is a function of  $u$ , such that as  $u$  varies from 0 to 1, each  $\lambda_m(u)$  also varies from 0 to 1, and  
 19 the path  $P$  defining the changes in anthropogenic emissions is traced from the background case  
 20 to the base case in the  $M$ -dimensional space of the scaling parameters  $\lambda_m$ . However,  $u$  may not  
 21 equal the normalized distance along  $P$ , denoted by  $s$ , and  $s$  can be useful in designing the  
 22 numerical integration procedure because it is easier to understand the distribution of the  
 23 integration points using  $s$ . The absolute distance  $D$  is related to  $u$  by

$$25 \quad D(u) = \int_0^u \left[ \sum_{m=1}^M \left( \frac{d\lambda_m}{du} \right)^2 \right]^{1/2} du$$

24

(3)

26 Then,  $s(u) = D(u)/D(1)$ . Changing the integration variable from  $u$  to  $s$ , the source contribution  
 27 becomes

$$28 \quad S_{im}(\mathbf{x}, t; P) = \int_0^1 \frac{\partial c_i(\mathbf{x}, t; \Lambda)}{\partial \lambda_m} \Big|_{\Lambda=\Lambda(s)} \frac{d\lambda_m}{ds} ds$$

1 (4)

2 with

$$4 \quad \frac{d\lambda_m}{ds} = \frac{d\lambda_m}{du} \frac{D(1)}{\left[ \sum_{m=1}^M \left( \frac{d\lambda_m}{du} \right)^2 \right]^{1/2}}$$

3 (5)

5 The sensitivity in Eq. (4) is evaluated along the specific path defined by  $\Lambda(s)$ . Also, though the  
6 emissions are reduced along the path and the concentrations are determined in a simulation with  
7 the reduced emissions, the sensitivity of  $c_i$  is to  $\lambda_m$ , which scales the full emissions in the base  
8 case, not the reduced emissions. The decoupled direct method (DDM) provides an accurate,  
9 efficient means for calculating the sensitivities (Dunker, 1981, 1984; Yang et al., 1997). The  
10 DDM has been implemented in current 3-D models for the formation of O<sub>3</sub> and particulate  
11 matter (Dunker et al., 2002a; Cohan et al., 2005; Napelenok et al., 2006; Koo et al., 2007).

12 The simplest and shortest integration path, termed the diagonal path, is defined by  $\lambda_m(u) = u$ ,  
13 all  $m$ . This is a straight line from  $\Lambda = 0$  to  $\Lambda = 1$  along which the emissions from all sources  
14 are reduced or grown by the common factor  $\lambda_m(u) = u$ . If there are two sources, Fig. 1 displays  
15 the diagonal path, Path 1, and two other possible paths. Path 2 is defined by the equations:

$$16 \quad \lambda_1(u) = u^3 \tag{6}$$

$$17 \quad \lambda_2(u) = \sin\left(\pi \frac{u}{2}\right) \tag{7}$$

18 Beginning at the base case, point B, emissions from source 1 are reduced much more rapidly  
19 than those from source 2 along Path 2. As the first 80% of the emissions from source 1 are  
20 reduced, only 20% of the emissions from source 2 are reduced. Then the remaining 80% of the  
21 emissions from source 2 are reduced as the remaining 20% of the emissions from source 1 are  
22 reduced, down to the background case, point b. Path 3 is the opposite of Path 2, obtained by  
23 interchanging the definitions of  $\lambda_1$  and  $\lambda_2$  in Eqs. (6, 7). For the diagonal path, the normalized  
24 distance and path variable are identical,  $s(u) = u$ , and  $d\lambda_m/ds$  in Eq. (4) is identically 1. For  
25 Paths 2 and 3,  $s(u) \neq u$ , and  $d\lambda_m/ds$  must be determined from Eq. (5).

26 The Gaussian numerical integration formulas have maximum precision (Isaacson and Keller,  
27 1966). This means that for a given number of points at which the integrand is evaluated,  $n$ , the  
28 formulas give an exact integration of all polynomials of degree 0 up to  $2n-1$ , the maximum

1 degree possible using  $n$  points. Thus, the Gaussian formulas should minimize the number of  
 2 points at which the integrand in Eq. (4) must be evaluated to achieve a given accuracy. This is  
 3 useful because the major computational effort in the PIM is determining the sensitivities at  
 4 multiple points along the path  $P$ . The Gauss-Legendre formula is one version of Gaussian  
 5 integration suited to integration of a function  $f(z)$  over a finite interval:

$$7 \int_a^b f(z) dz \cong \frac{b-a}{2} \sum_{k=1}^n w(\xi_k) f\left(\frac{b-a}{2} \xi_k + \frac{b+a}{2}\right)$$

6 (8)

$$9 z = \frac{b-a}{2} \xi + \frac{b+a}{2}$$

8 (9)

10 The  $\xi_k$  are the zeroes of the Legendre polynomials, and the  $w(\xi_k)$  are weights determined to give  
 11 the formula the maximum precision. The  $\xi_k$  and  $w(\xi_k)$  are readily available (efunda, 2014).

## 12 2.2 Special cases

13 One special case is successive zero-out (SZO) of the sources. In SZO, the emissions from one  
 14 source are reduced to zero while leaving all other emissions unchanged, then the emissions  
 15 from a second source are reduced to zero, etc. until the background case is reached. This is a  
 16 path along the edges of a hypercube in  $\Lambda$ -space. (The hypercube defines all possible emission-  
 17 control strategies, contains  $M$  axes, one axis for each  $\lambda_m$ , and includes all values of  $\lambda_m$  from 0 to  
 18 1.) In Fig. 1, one SZO path would be  $B$ - $b_2$ - $b$  and the other,  $B$ - $b_1$ - $b$ . Along the segment  $B$  to  $b_2$   
 19 of the former path, the sensitivities are nonzero, but  $d\lambda_2 = 0$ . Therefore, the only contribution  
 20 to  $\Delta c_i$  in Eq. (1) is that for source 1, and this contribution equals  $c_i^B - c_i^{b_2}$ . Similarly, along the  
 21 segment from  $b_2$  to  $b$ ,  $d\lambda_1 = 0$ , the only contribution to  $\Delta c_i$  is that for source 2, and the  
 22 contribution equals  $c_i^{b_2} - c_i^b$ . Thus, a SZO path is a special case of PIM in which no calculation  
 23 or integration of sensitivities is required, only a series of simulations to obtain the  
 24 concentrations at the corners of the hypercube. Calculation and integration of the sensitivities  
 25 is necessary if two or more sources are controlled simultaneously, and the path is then interior  
 26 to the hypercube.

1 Another special case involves expanding the sensitivities in a Taylor series in the  $\lambda_m$  at  $\Lambda = 1$   
 2 (base case). If there are two sources and the Taylor series through first order in  $\lambda_m$  is integrated  
 3 along the diagonal path, then (see Supplementary Information (SI))

$$5 \quad S_{i1}(diag) = \left. \frac{\partial c_i}{\partial \lambda_1} \right|_{\Lambda=1} - \frac{1}{2} \left. \frac{\partial^2 c_i}{\partial \lambda_1^2} \right|_{\Lambda=1} - \frac{1}{2} \left. \frac{\partial^2 c_i}{\partial \lambda_1 \partial \lambda_2} \right|_{\Lambda=1}$$

4 (10)

$$7 \quad S_{i2}(diag) = \left. \frac{\partial c_i}{\partial \lambda_2} \right|_{\Lambda=1} - \frac{1}{2} \left. \frac{\partial^2 c_i}{\partial \lambda_2^2} \right|_{\Lambda=1} - \frac{1}{2} \left. \frac{\partial^2 c_i}{\partial \lambda_1 \partial \lambda_2} \right|_{\Lambda=1}$$

6 (11)

8 The cross term (  $-\partial^2 c_i / \partial \lambda_1 \partial \lambda_2$  ) is split evenly between  $S_{i1}$  and  $S_{i2}$ . If the integration is done  
 9 instead on the path  $B-b1-b$  in Fig. 1, the full cross term is assigned to  $S_{i1}$  and is absent entirely  
 10 from  $S_{i2}$ . Similarly, if the integration is along the path  $B-b2-b$ , the full cross term is assigned to  
 11  $S_{i2}$  and is absent from  $S_{i1}$ . Thus, the source contributions are the same for these 3 paths except  
 12 for the location of the cross term. Cohan et al. (2005) expanded  $c_i$  in a second-order Taylor  
 13 series about  $\Lambda = 1$  and used it to develop source apportionments that are the same as Eqs. (10,  
 14 11) except that they did not assign the cross term to the individual sources. The PIM shows  
 15 that the cross term can be assigned to sources based on the emission-control path.

### 16 2.3 Analogy in thermodynamics

17 The dependence of the source contributions on path has an analogy in thermodynamics. For  
 18 example, in the case of a single-component gas, the energy  $E$  is a function of the state variables:  
 19 temperature  $T$ , and volume  $V$ . The change in  $E$  between two states of the system,  $\Delta E$ , depends  
 20 only on the initial and final values of  $T$  and  $V$ . However, when  $\Delta E$  is split into contributions  
 21 from the heat exchange with the surroundings (  $\int_p dq$  ) and the pressure ( $p$ )-related work  
 22 (  $\int_p p dV$  ) in the equation,  $\Delta E = \int_p dq - \int_p p dV$ , the heat exchange and work depend on  
 23 the path  $P$  from the initial to final states of the system. Thus, the concentrations  $c_i$  from an air  
 24 quality simulation may be regarded as analogous to  $E$  and the emissions, initial and boundary  
 25 concentrations, meteorology and chemical mechanism as analogous to  $T$  and  $V$ . The  $\Delta c_i$   
 26 between two simulations differing only in emissions can be allocated to sources, but this  
 27 allocation is analogous to heat exchange and work and depends on the path along which the  
 28 emissions are changed.



1

### 2 **3 Model and inputs**

3 Time-dependent inputs were developed for CAMx, v6.00, configured with 2 cells in a vertical  
4 column. The lower cell varied diurnally in height from 100 →300 →100 m and the upper cell  
5 varied in height such that the top of the column was 1500 m. Diurnally varying emissions were  
6 introduced at the bottom boundary. The simulations were run for 3 days, June 20-22, beginning  
7 with clean initial concentrations in both cells. There was no transport into the cells via the  
8 lateral or top boundaries. The latitude was that of Los Angeles and Atlanta. The Carbon Bond  
9 6 (CB6) chemical mechanism represented the gas-phase chemistry (Yarwood et al., 2012). The  
10 effect of the inputs is that cleaner air from the upper cell is entrained into the lower cell during  
11 the morning as the lower cell grows in height. Then, in the evening, the lower cell shrinks in  
12 height and leaves pollutants aloft in the upper cell. Consequently, there is carry-over of  
13 pollutants from day to day affecting the chemistry in the lower cell. Additional details of the  
14 simulations are in Table S1 (SI).

15 The emissions were developed from the national totals in the 2008 U.S. National Emission  
16 Inventory, version 3 (U.S. EPA, 2013b) with several adjustments. Emissions from wildfires  
17 and prescribed fires were excluded because these vary greatly from year to year and were  
18 unusually high in 2008. Also, to represent summer conditions, emissions from residential wood  
19 combustion were excluded. Further, emissions of NO from lightning were added (Koo et al.,  
20 2010). The emissions were segregated into biogenic (plus lightning) emissions and 5 major  
21 source categories of anthropogenic emissions: fuel combustion, industrial sources, on-road  
22 vehicles, non-road vehicles, and other emissions. Vegetation and soil emissions and their  
23 speciation are from BEIS3.14 (Pierce et al., 1998). Anthropogenic emissions of volatile organic  
24 compounds (VOC's) from a major source category were allocated to CB6 species using  
25 speciation profiles from SPECIATE 4.3 for 1 or 2 sub-categories of sources comprising a  
26 significant fraction of the VOC emissions (Simon et al., 2010; U.S. EPA, 2013a). The annual  
27 emissions of VOC species, NO<sub>x</sub> (=NO + NO<sub>2</sub>), CO, and HONO for each source category were  
28 allocated to hours of a Wednesday in June using temporal profiles (U.S. EPA, 2013c). On a  
29 national scale, the biogenic VOC emissions are large compared to the anthropogenic VOC  
30 emissions, but this is not the case in urban areas. To represent better an urban area the  
31 anthropogenic emissions were weighted by a factor of 5 and the biogenic emissions by a factor

1 of 1. A summary of the resulting daily emission rates for all source categories is given in Table  
2 1, and the complete set of emission rates is in Table S2.

3 The model and inputs are not intended to be a detailed representation of a specific urban area  
4 but rather to provide a useful platform for testing the PIM, specifically different integration  
5 formulas and the dependence of the source contributions on paths.

6

## 7 **4 Results**

8 The concentrations of O<sub>3</sub> and formaldehyde (FORM) in the background simulation (biogenic  
9 emissions only), the base simulation (both the biogenic and anthropogenic emissions) and the  
10 difference between the simulations (anthropogenic increment) are shown in Fig. 2. Similar  
11 plots for NO<sub>2</sub> and HNO<sub>3</sub> are in Fig. S1. The peak O<sub>3</sub> concentration remains relatively constant  
12 over the 3 days in the background simulation (47-52 ppb) but increases steadily in the base  
13 simulation (from 75 ppb on day 1 to 151 ppb on day 3) due to the additional anthropogenic  
14 emissions on days 2 and 3 and the carryover of pollutants in the upper cell. Both O<sub>3</sub> and FORM  
15 have sizeable concentrations in the background case whereas NO<sub>2</sub> and HNO<sub>3</sub> have very low  
16 concentrations due to the low biogenic NO<sub>x</sub> emissions. The O<sub>3</sub> increment is negative at the  
17 beginning of day 1 due to the titration of O<sub>3</sub> by the anthropogenic NO emissions. The VOC/NO<sub>x</sub>  
18 ratio in the base case increases from 5-7 on day 1 to 9-20 ppbC/ppb<sup>-1</sup> on day 3. Overall, the  
19 simulations provide a wide range of conditions for testing the PIM.

### 20 **4.1 Accuracy of the numerical integration**

21 The O<sub>3</sub>, FORM, NO<sub>2</sub>, and HNO<sub>3</sub> increments were allocated to the 5 anthropogenic source  
22 categories and to the 4 species or groups of species emitted by each source category: VOC, CO,  
23 NO<sub>x</sub>, and HONO. Thus, a total of  $M = 20$  sensitivities were calculated and integrated in the  
24 PIM. Source apportionments were determined for 3 emission-control paths: diagonal (Diag);  
25 VOC first (VOCF); NO<sub>x</sub> first (NOxF). Along the Diag path, the scaling parameters  $\lambda_m^{VOC} =$   
26  $\lambda_m^{CO} = \lambda_m^{NOx} = \lambda_m^{HONO} = u$ , for each source category  $m = 1, \dots, 5$ . Thus, the sources and  
27 emission species are treated equivalently. The VOCF path emphasizes initial control of VOC  
28 and CO emissions followed by later control of NO<sub>x</sub> and HONO emissions, as defined by  $\lambda_m^{VOC}$   
29  $= \lambda_m^{CO} = u^3$  and  $\lambda_m^{NOx} = \lambda_m^{HONO} = \sin(\pi u/2)$ ,  $m = 1, \dots, 5$ . The NOxF path has the reverse  
30 assignments of  $u^3$  and  $\sin(\pi u/2)$ . Viewing  $\lambda_m^{VOC}$ ,  $\lambda_m^{CO}$  as analogous to  $\lambda_l$  in Fig. 1 and  $\lambda_m^{NOx}$ ,

1  $\lambda_m^{HONO}$  as analogous to  $\lambda_2$ , , then the VOcF path in 20-dimensional space is analogous to Path  
 2 2 in Fig. 1 and the NOx F path is analogous to Path 3.

3 The Gauss-Legendre formula was tested for accuracy using different numbers of integration  
 4 points and different integration variables. One set of tests, labeled GLns, used the distance  $s$  as  
 5 the integration variable and  $n$  integration points. Another set of tests, labeled GLnr, used a  
 6 transformation of the variable  $s$  to  $r = s^{1/2}$ . Equation (4) then becomes

$$8 \quad S_{im}(\mathbf{x}, t; P) = 2 \int_0^1 \frac{\partial c_i(\mathbf{x}, t; \Lambda)}{\partial \lambda_m} \Big|_{\Lambda=\Lambda(s[r])} \frac{d\lambda_m}{ds} \Big|_{s(r)} r dr$$

7 (12)

9 Because the background case contains no anthropogenic emissions, O<sub>3</sub> formation is strongly  
 10 limited by the availability of NO<sub>x</sub>. As a consequence, the sensitivity of O<sub>3</sub> with respect to any  
 11  $\lambda_m$  that scales NO<sub>x</sub> emissions is very large near  $\Lambda = 0$ , but the sensitivity decreases very rapidly  
 12 as NO<sub>x</sub> emissions are added. The transformation to  $r$  has two potentially beneficial effects for  
 13 the source apportionment of O<sub>3</sub>. First, the points for the numerical integration are chosen for  
 14 the variable  $r$ . When transformed back to the variable  $s$ , the points for  $s$  are closer to  $\Lambda = 0$   
 15 than if  $s$  were the integration variable, giving more resolution where the sensitivity is changing  
 16 most rapidly. Second, the factor  $r$  in Eq. (12) reduces the magnitude of the integrand near  $r =$   
 17  $s = \lambda_m = 0$ , and makes the integrand identically 0 at  $r = 0$ . This can yield an integrand that is  
 18 easier to integrate. Finally, as a simple alternative, the source contributions were calculated by  
 19 the trapezoidal rule using the 2 points at  $\Lambda = 0$  and 1 (labeled TR2).

20 The sum of the source contributions on the 3 paths was compared to the anthropogenic  
 21 concentration increment (right- vs. left-hand sides of Eq. (1)) to determine the accuracy of the  
 22 formulas. Table 2 gives the mean absolute error and mean bias of the formulas for O<sub>3</sub> and  
 23 FORM, and Table S3 gives the error and bias for NO<sub>2</sub> and HNO<sub>3</sub>. For comparison, the mean  
 24 absolute values of the increments  $\Delta O_3$ ,  $\Delta FORM$ ,  $\Delta NO_2$ , and  $\Delta HNO_3$  are 34.9 ppb, 1.52 ppb,  
 25 7.67 ppb, and 16.0 ppb, respectively. Though they use the same number of points, there is a  
 26 large reduction in error and bias from TR2 to GL2s or GL2r, indicating the significant  
 27 advantage of the GL formulas. As the number of points included in the GLns or GLnr formulas  
 28 increases, the error decreases for O<sub>3</sub>, FORM, and NO<sub>2</sub> and generally the bias as well. There are  
 29 some exceptions to this trend for HNO<sub>3</sub>, but these occur for cases where the error and bias are  
 30 already quite low (average error < 4% of the average increment). For O<sub>3</sub> and the Diag path, the

1 GLnr formula gives more accurate results than the GLns formula for 2 or 3 points and  
2 essentially the same accuracy for 4 points. For FORM, the GLnr formula is always more  
3 accurate than the GLns formula. The GLnr formula is usually less accurate than the GLns  
4 formula for NO<sub>2</sub> and HNO<sub>3</sub> and for O<sub>3</sub> with the NO<sub>x</sub>F and VO<sub>CF</sub> paths.

5 Table 2 also shows that the accuracy of a formula is lower for the VO<sub>CF</sub> path than the other  
6 paths when using the same number of points. This difference can be understood by examining  
7 the integrand in Eq. (4). Figure 3 displays the integrands for allocating ΔO<sub>3</sub> to sources at the  
8 time of peak O<sub>3</sub> on day 3, when it is most difficult to obtain good agreement between the sum  
9 of the source contributions and ΔO<sub>3</sub>. Along the Diag and NO<sub>x</sub>F paths, the integrands have a  
10 constant curvature, either positive (Diag) or negative (NO<sub>x</sub>F), and the integrands are mainly  
11 positive, with only small negative values near  $s = 1$ . However, along the VO<sub>CF</sub> path, 4 of the  
12 integrands have positive curvature from  $s = 0$  to  $s = \sim 0.5$  and then negative curvature for the  
13 remainder of the path. Also, the integrands vary over a wider range along the VO<sub>CF</sub> path than  
14 the other paths. Further, the integrands for on-road vehicles and fuel combustion are both  
15 positive and negative, resulting in the cancellation of contributions to the integrals from  
16 different sections of the path. The change in curvature, wider range of variation and especially  
17 the cancellation of contributions require more points on the VO<sub>CF</sub> path to obtain an accurate  
18 integration.

19 Overall, the GL3r formula for the Diag path and the GL4s formula for the other paths give quite  
20 accurate results and were used to calculate the source apportionments in Sect. 4.2. Figure S2  
21 gives a comparison of the sum of the source contributions vs. ΔO<sub>3</sub>, ΔFORM, ΔNO<sub>2</sub>, and ΔHNO<sub>3</sub>  
22 at each hour of the simulation. The plots show again that the largest errors occur for the VO<sub>CF</sub>  
23 path.

## 24 **4.2 Source apportionments**

25 Figure 4 presents the apportionment of ΔO<sub>3</sub> to the 5 source categories and 4 emission species  
26 using the Diag path. The VOC contributions are always positive, and the largest contributions  
27 are from industrial sources and on-road and non-road vehicles. The NO<sub>x</sub> contributions are small  
28 and primarily negative on day 1, when the atmospheric VOC/NO<sub>x</sub> < 7.5 ppbC/ppb<sup>-1</sup> in the base  
29 case. Under these conditions, NO<sub>x</sub> emissions tend to inhibit O<sub>3</sub> formation, and hence the  
30 contributions are negative. On day 2, however, the NO<sub>x</sub> contributions become positive and then  
31 increase from day 2 to day 3. The total of the NO<sub>x</sub> contributions from all sources at 42 h is

1 essentially the same as the total VOC contribution, and at 66 h, the total NO<sub>x</sub> contribution is  
2 twice the total VOC contribution. The increasing importance of the NO<sub>x</sub> contributions is due  
3 to the increasing VOC/NO<sub>x</sub>, which is 10-20 ppbC/ppb<sup>-1</sup> after 36 h, resulting in NO<sub>x</sub>-limited O<sub>3</sub>  
4 formation.

5 The PIM can separate the contributions of all emission species. Figure 4 shows that the CO  
6 contributions from on-road and non-road vehicles are not negligible compared to the VOC  
7 contributions of these sources. For on-road vehicles, the CO contributions are generally 20-  
8 45% of the VOC contributions, and for non-road vehicles, 10-30%. HONO emissions are  
9 assigned only to on-road and non-road vehicles and are small (0.8% of NO<sub>x</sub>, Table 1). For both  
10 of these sources, their HONO emissions contribute < 0.35 ppb to the ΔO<sub>3</sub>.

11 Figure 5 displays the source contributions to ΔO<sub>3</sub> obtained with the 3 paths. (The contributions  
12 of all emission species from a source are combined together.) Results for the Diag and NO<sub>x</sub>F  
13 path are similar. For these paths, on-road vehicles have the largest and non-road vehicles the  
14 second-largest contributions during most of the simulation, and the “other” category contributes  
15 <3 ppb to ΔO<sub>3</sub>. However, industrial sources are more important than fuel combustion for the  
16 Diag path and the reverse is true for the NO<sub>x</sub>F path. The source contributions for the VO<sub>x</sub>F  
17 path are distinctly different. Over most of the simulation, the ranking of the contributions is  
18 industrial sources > non-road vehicles > on-road vehicles, the opposite of the Diag path. Also,  
19 fuel combustion has a negative contribution over the entire simulation and the other category  
20 has a larger contribution (up to 6.5 ppb) than for the Diag and NO<sub>x</sub>F paths.

21 The different results for the VO<sub>x</sub>F path can be explained by the fact that the NO<sub>x</sub> emissions are  
22 controlled last on this path or, in terms of the integration, essentially only NO<sub>x</sub> emissions are  
23 added near  $s = 0$ . The sensitivity of O<sub>3</sub> to these emissions is large and positive near  $s = 0$  (Fig.  
24 3) because the VOC/NO<sub>x</sub> ratio is high in the background case. However, the VOC/NO<sub>x</sub> ratio  
25 decreases rapidly as  $s$  increases along the VO<sub>x</sub>F path, the sensitivity to NO<sub>x</sub> emissions becomes  
26 negative, and O<sub>3</sub> formation becomes VOC-limited for most of the path. Thus, fuel combustion  
27 has a negative source contribution because its emissions are mostly NO<sub>x</sub>, and industrial sources  
28 have the largest positive contribution because they have the largest VOC emissions. Also, non-  
29 road vehicles have a larger contribution than on-road vehicles because both sources have a  
30 similar magnitude of VOC emissions but on-road vehicles have 82% more NO<sub>x</sub> emissions,  
31 which suppress O<sub>3</sub> formation on the VOC-limited section of the path.

1 The source contributions to  $\Delta\text{FORM}$  for the 3 paths are also in Fig. 5. For the Diag path, the  
2 relative importance of the sources on days 2 and 3 is the same for  $\Delta\text{FORM}$  as for  $\Delta\text{O}_3$ , and this  
3 is also true for the  $\text{NO}_x\text{F}$  path. For the  $\text{VOCF}$  path, the on-road and non-road vehicles  
4 contribute more to  $\Delta\text{FORM}$  than the industrial sources, but the reverse is true for the  
5 contributions of these sources to  $\Delta\text{O}_3$ . The on-road and non-road vehicles have the largest  
6 contributions to  $\Delta\text{FORM}$  on each path because these sources have the largest primary  $\text{FORM}$   
7 emissions and the largest emissions of olefins, which are important precursors to secondary  
8  $\text{FORM}$  from oxidation reactions (Table S2).

9 Figure S3 contains the apportionment of  $\Delta\text{NO}_2$  and  $\Delta\text{HNO}_3$  to sources. The source  
10 contributions to  $\Delta\text{NO}_2$  for the Diag and  $\text{NO}_x\text{F}$  paths are quite similar; those for the  $\text{VOCF}$  path  
11 differ in that the contributions of the industrial sources and other category are primarily negative  
12 after 18 h. The source contributions to  $\Delta\text{HNO}_3$  for the Diag and  $\text{NO}_x\text{F}$  paths are again quite  
13 similar, and the ranking of the sources in importance is the same as the ranking of their  $\text{NO}_x$   
14 emissions. The source contributions to  $\Delta\text{HNO}_3$  for the  $\text{VOCF}$  path are similar to those for the  
15 other paths except that the contributions of non-road vehicles and fuel combustion are reversed  
16 in importance. The reversal is likely due to the much larger  $\text{VOC}$  emissions from non-road  
17 vehicles, which would enhance the oxidation of  $\text{NO}_x$  on the  $\text{VOC}$ -limited part of the path.

18

## 19 **5 Conclusions**

20 As shown in Sect. 4, the PIM can allocate the difference in concentration between two  
21 simulations to emission sources. Consequently, the PIM requires that the base-case  
22 concentration minus the sum of the anthropogenic source contributions (difference  $\delta$ ) equals  
23 the background concentration (within the accuracy of the numerical integration). Other  
24 methods do not have this constraint. If  $\delta$  is less than the background concentration, then the  
25 method assigns too much importance to the anthropogenic sources and will give the impression  
26 that reducing anthropogenic emissions will reduce the pollutant concentration more than will  
27 actually occur (over-allocation of the anthropogenic increment to the anthropogenic sources).  
28 Similarly, if  $\delta$  is greater than the background concentration, the method assigns too little  
29 importance to the anthropogenic sources (under-allocation of the anthropogenic increment).  
30 The PIM ensures that the anthropogenic increments to  $\text{O}_3$  and the other species are neither over-  
31 nor under-allocated to the anthropogenic sources.

1 Another advantage is that the PIM is based on an exact mathematical relationship that is  
2 independent of the chemistry or model and does not require added relationships or  
3 approximations. The PIM allows source contributions to be either positive or negative. If the  
4 secondary pollutant formation is inhibited by emissions of some species, source, or geographic  
5 area, the sensitivity to these emissions will be negative for at least some values of the scaling  
6 parameter  $\lambda_m$ , and the integral in Eq. (2) may be negative.

7 Once a model has been modified to calculate the first-order sensitivities, the PIM requires only  
8 very simple post-processing of model results, specifically, calculating a linear combination of  
9 sensitivities from different simulations. This can be readily done with existing post-processing  
10 packages such as the Package for Visualization of Environmental data (PAVE) or the  
11 Visualization Environment for Rich Data Interpretation (VERDI) (Univ. of North Carolina,  
12 2004, 2014). The PIM is not focused on just one species, e.g., O<sub>3</sub>. The calculations needed to  
13 allocate  $\Delta c_i$  for species  $i$  also generate all the information needed to allocate  $\Delta c_j$  for any other  
14 species  $j$  predicted by the model, and there is minimal additional effort needed to allocate  $\Delta c_j$   
15 for the second and subsequent species. Finally, the PIM highlights the importance of the  
16 background simulation. For a simulation with anthropogenic emissions included to be useful  
17 in designing emission controls, there is an implicit assumption that a simulation without the  
18 anthropogenic emissions gives concentrations consistent with estimates for clean air. The  
19 concentration in the background simulation can be determined by an actual simulation or by  
20 subtracting the sum of all the source contributions from the base-case concentration.

21 In principle, there is an infinite number of source apportionments available from the PIM.  
22 However, each source apportionment is linked to an emission-control strategy. If a control  
23 strategy is defined along with the timing of the controls, the number of source apportionments  
24 is reduced to just one.

25 The major disadvantage of the PIM is that it requires more computational effort than other  
26 methods because the sensitivities must be determined at several emission levels between the  
27 base and background simulations. This disadvantage is mitigated, to some degree, because the  
28 additional simulations provide information on how concentrations and sensitivities will change  
29 along the emission-control path.

30 The PIM has been applied in this work to a simplified configuration of CAMx that includes the  
31 nonlinear chemistry but not transport or dispersion. However, transport and dispersion do not  
32 involve nonlinear interactions among the species. Because the nonlinear dependence of the

1 sensitivities on the integration variable (Fig. 3) is driven by the nonlinear chemistry and a full  
2 3-D configuration should not have any other sources of nonlinearity, the number of integration  
3 points required for PIM for a 3-D configuration should be similar to the number required for  
4 the simplified configuration (3 or 4) (Dunker et al., 2015).

5

## 6 **Supplementary information**

7 Application of the PIM to the special case involving the Taylor series expansion, input data and  
8 emissions for the model simulations, accuracy in allocating  $\Delta\text{NO}_2$  and  $\Delta\text{HNO}_3$  to sources using  
9 different integration formulas, comparison of the sum of the source contributions to the  
10 anthropogenic increment at each hour, and source contributions to  $\Delta\text{NO}_2$  and  $\Delta\text{HNO}_3$ .

11



## 1 **References**

- 2 Bowman F. M.: A multi-parent assignment method for analyzing atmospheric chemistry  
3 mechanisms, *Atmos. Environ.*, 39, 2519-2533, 2005.
- 4 Bowman, F. M. and Seinfeld, J. H.: Ozone productivity of atmospheric organics. *J. Geophys.*  
5 *Res.*, 99, 5309-5324, 1994.
- 6 Butler, T. M., Lawrence, M. G., Taraborrelli, D., and Lelieveld, J.: Multi-day ozone production  
7 potential of volatile organic compounds calculated with a tagging approach, *Atmos. Environ.*,  
8 45, 4082-4090, 2011.
- 9 Cohan D. S., Hakami A., Hu, Y., and Russell A. G.: Nonlinear response of ozone to emissions:  
10 source apportionment and sensitivity analysis, *Environ. Sci. Technol.*, 39, 6739-6748, 2005.
- 11 Dunker, A.M.: Efficient calculation of sensitivity coefficients for complex atmospheric models.  
12 *Atmos. Environ.*, 15, 1155-1161, 1981.
- 13 Dunker, A. M.: The decoupled direct method for calculating sensitivity coefficients in chemical  
14 kinetics, *J. Chem. Phys.*, 81, 2385-2393, 1984.
- 15 Dunker, A. M., Yarwood, G., Ortmann, J. P., and Wilson, G. M.: The decoupled direct method  
16 for sensitivity analysis in a three-dimensional air quality model- implementation, accuracy, and  
17 efficiency, *Environ. Sci. Technol.*, 36, 2965-2976, 2002a.
- 18 Dunker, A. M., Yarwood, G., Ortmann, J. P., and Wilson, G. M.: Comparison of source  
19 apportionment and source sensitivity of ozone in a three-dimensional air quality model,  
20 *Environ. Sci. Technol.*, 36, 2593-2964, 2002b.
- 21 Dunker, A. M., Koo, B., and Yarwood, G.: Source apportionment of the anthropogenic  
22 increment to ozone, formaldehyde, and nitrogen dioxide by the path-integral method in a 3-D  
23 model, *Environ. Sci. Technol.*, [dx.doi.org/10.1021/acs.est.5b00467](https://doi.org/10.1021/acs.est.5b00467), 2015.
- 24 efunda: available at [http://www.efunda.com/math/num\\_integration/findgausslegendre.cfm](http://www.efunda.com/math/num_integration/findgausslegendre.cfm)  
25 (last access: 29 January 2014), 2014.
- 26 Emmons, L. K., Hess, P. G., Lamarque, J.-F., and Pfister, G. G.: Tagged ozone mechanism for  
27 MOZART-4, CAM-chem and other chemical transport models, *Geosci. Model Dev.*, 5, 1531-  
28 1542, 2012.

1 ENVIRON: Comprehensive Air Quality Model with Extensions, available at;  
2 <http://www.CAMx.com> (last access: 15 May 2013), 2013.

3 Grewe, V.: A generalized tagging method, *Geosci. Model Dev.*, 6, 247-253, 2013.

4 Grewe, V., Tsati, E., and Hoor, P.: On the attribution of contributions of atmospheric trace gases  
5 to emissions in atmospheric model applications, *Geosci. Model Dev.*, 3, 487-499, 2010.

6 Isaacson, E. and Keller, H. B.: *Analysis of Numerical Methods*, John Wiley, New York, 1966.

7 Kaplan, W.: *Advanced Calculus*, Addison-Wesley, Reading, Massachusetts, 1959.

8 Koo, B., Dunker, A. M., and Yarwood, G.: Implementing the decoupled direct method for  
9 sensitivity analysis in a particulate matter air quality model, *Environ. Sci. Technol.*, 41, 2847-  
10 2854, 2007.

11 Koo, B., Wilson, G. M., Morris, R. E., Dunker, A. M., and Yarwood, G.: Comparison of source  
12 apportionment and sensitivity analysis in a particulate matter air quality model, *Environ. Sci.*  
13 *Technol.*, 43, 6669-6675, 2009.

14 Koo, B., Chien, C.-J., Tonnesen, G., Morris, R., Johnson, J., Sakulyanontvittaya, T.,  
15 Piyachaturawat, P., and Yarwood, G.: Natural emissions for regional modeling of background  
16 ozone and particulate matter and impacts on emissions control strategies, *Atmos. Environ.* 44,  
17 2372-2382, 2010.

18 Kwok, R. H. F., Napelenok, S. L., and Baker, K. R.: Implementation and evaluation of PM<sub>2.5</sub>  
19 source contribution analysis in a photochemical model, *Atmos. Environ.*, 80, 398-407, 2013.

20 Marmur, A., Park, S.-K., Mulholland, J. A., Tolbert, P. E., and Russell, A. G.: Source  
21 apportionment of PM<sub>2.5</sub> in the southeastern United States using receptor and emissions-based  
22 models: conceptual differences and implications for time-series health studies, *Atmos.*  
23 *Environ.*, 40, 2533-2551, 2006.

24 Mysliwiec, M. J. and Kleeman M. J.: Source apportionment of secondary airborne particulate  
25 matter in a polluted atmosphere, *Environ. Sci. Technol.*, 36, 5376-5384, 2002.

26 Napelenok, S. L., Cohan D. S., Hu, Y., and Russell A. G.: Decoupled direct 3D sensitivity  
27 analysis for particulate matter (DDM-3D/PM), *Atmos. Environ.*, 40, 6112-6121, 2006.

1 Pierce, T., Geron, C., Bender, L., Dennis, R., Tonnesen, G., and Guenther, A.: Influence of  
2 increased isoprene emissions on regional ozone modeling, *J. Geophys. Res.*, 103, 25611-25629,  
3 1998.

4 Simon, H., Beck, L., Bhave, P.V., Divita, F., Hsu, Y., Luecken, D., Mobley, J.D., Pouliot, G.A.,  
5 Reff, A., Sarwar, G., and Strum, M.: The development and uses of EPA's SPECIATE database,  
6 *Atmospheric Pollution Research*, 1, 196-206, 2010.

7 Stein, U. and Alpert, P.: Factor separation in numerical simulations, *J. Atmos. Sci.*, 50, 2107-  
8 2115, 1993.

9 Tao, Z., Larson S. M., Williams A., Caughey, M. and Wuebbles D. J.: Area, mobile, and point  
10 source contributions to ground level ozone: a summer simulation across the continental USA,  
11 *Atmos. Environ.*, 39, 1869-1877, 2005.

12 Tong, D. Q. and Mauzerall, D. L.: Summertime state-level source-receptor relationships  
13 between nitrogen oxides emissions and surface ozone concentrations over the continental  
14 United States, *Environ. Sci. Technol.*, 42, 7976-7984, 2008.

15 University of North Carolina, Package for Analysis and Visualization of Environmental Data,  
16 version 2.3, available at:  
17 [http://www.ie.unc.edu/cempd/EDSS/pave\\_doc/EntirePaveManual.html](http://www.ie.unc.edu/cempd/EDSS/pave_doc/EntirePaveManual.html) (last access: 17  
18 November 2014), 2004.

19 University of North Carolina, Visualization Environment for Rich Data Interpretation, version  
20 1.5, available at: <https://www.cmascenter.org/verdi/> (last access: 17 November 2014), 2014.

21 U.S. EPA: Carbon Bond and SAPRC Speciation Profiles, available at:  
22 <http://www.cmascenter.org/download/data.cfm> (last access: 19 November 2013), 2013a.

23 U.S. EPA: 2008 National Emissions Inventory, Version 3, Technical Support Document,  
24 September 2013-Draft, available at: <http://www.epa.gov/ttn/chief/net/2008inventory.html> (last  
25 access: 20 November 2013), 2013b.

26 U.S. EPA: CAIR Platform Data, available at:  
27 <http://www.epa.gov/ttn/chief/emch/temporal/index.html> (last access: 24 December 2013),  
28 2013c.

1 Wagstrom, K. M., Pandis, S. N., Yarwood, G., Wilson, G. M. and Morris, R. E.: Development  
2 and application of a computationally efficient particulate matter apportionment algorithm in a  
3 three-dimensional chemical transport model, *Atmos. Environ.*, 42, 5650-5659, 2008.

4 Wang, H., Jacob, D. J., LeSager, P., Streets, D. G., Park, R. J., Gilliland, A. B., and van  
5 Donkelaar, A.: Surface ozone background in the United States: Canadian and Mexican  
6 pollution influences, *Atmos. Environ.*, 43, 1310-1319, 2009.

7 Wang, Z. S., Chien, C. J. and Tonnesen, G. S.: Development of a tagged species source  
8 apportionment algorithm to characterize three-dimensional transport and transformation of  
9 precursors and secondary pollutants, *J. Geophys. Res.*, 114, D21206, doi:  
10 10.1029/2008JD010846, 2009.

11 Yang, Y-J., Wilkinson, J. G. and Russell, A. G.: Fast, direct sensitivity analysis of  
12 multidimensional photochemical models, *Environ. Sci. Technol.*, 31, 2859-2868, 1997.

13 Yarwood, G., Morris, R. E., Yocke, M. A., Hogo, H. and Chico, T. Development of a  
14 methodology for source apportionment of ozone concentration estimates from a photochemical  
15 grid model, in: *Proceedings of the 89th Annual Meeting of the Air & Waste Management*  
16 *Association*, Air and Waste Management Association, Pittsburgh, PA, Paper 96-TA23A.06,  
17 1996.

18 Yarwood, G., Gookyoung H., Carter, W.P.L., and Whitten, G.Z.: *Environmental Chamber*  
19 *Experiments to Evaluate NO<sub>x</sub> Sinks and Recycling in Atmospheric Chemical Mechanisms*,  
20 *Texas Air Quality Research Program Project 10-042*, University of Texas, Austin, 2012.

21 Zhang, Y., Wang, W., Wu, S.-Y., Wang, K., Minoura, H. and Wang, Z. Impacts of updated  
22 emission inventories on source apportionment of fine particle and ozone over the southeastern  
23 U.S., *Atmos. Environ.*, 88, 133-154, 2014.

24

1 Table 1. Summary of daily emission rates used in the base-case simulation.

Species	Emission Rate (mol day <sup>-1</sup> km <sup>-2</sup> )					
	Biogenic Sources <sup>a</sup>	Fuel Combustion	Industrial Sources	On-road Vehicles	Non-road Vehicles	Other Sources
NO	13.5	77.4	19.7	132.9	73.2	1.9
NO <sub>2</sub>	0.00	8.60	2.19	13.59	7.48	0.21
HONO	0.00	0.00	0.00	1.18	0.65	0.00
CO	35.9	51.8	58.2	1158.4	683.0	57.0
VOC	166.8	6.1	244.3	129.9	115.1	59.3
VOC/NO <sub>x</sub> <sup>b</sup>	29.8	0.09	16.6	1.4	2.4	31.8

2 <sup>a</sup> Includes lightning

3 <sup>b</sup> NO<sub>x</sub> = NO + NO<sub>2</sub>. VOC/NO<sub>x</sub> units are mole C (mole NO<sub>x</sub>)<sup>-1</sup>

4

1 Table 2. Average error and bias for different numerical integration formulas. The sum of the  
 2 source contributions calculated using the formula is compared to the anthropogenic increment  
 3 of O<sub>3</sub> or FORM.

Path	Formula <sup>a</sup>	Mean Absolute Error <sup>b</sup> (ppb)	Mean Bias <sup>b</sup> (ppb)
O <sub>3</sub> Increment			
Diag	TR2	65.93	65.93
Diag	GL2s	7.38	-7.36
Diag	GL2r	5.95	5.71
Diag	GL3s	3.32	-3.30
Diag	GL3r	1.64	-1.49
Diag	GL4s	1.51	-1.50
Diag	GL4r	1.54	-1.49
NOxF	GL3s	2.20	2.15
NOxF	GL3r	7.73	-7.67
NOxF	GL4s	1.57	-1.54
VOCF	GL3s	7.56	-7.32
VOCF	GL3r	10.46	9.62
VOCF	GL4s	4.68	-4.63
FORM Increment			
Diag	TR2	2.45	2.45
Diag	GL2s	0.21	-0.20
Diag	GL2r	0.19	0.19
Diag	GL3s	0.12	-0.12

Diag	GL3r	0.04	0.02
Diag	GL4s	0.05	-0.04
Diag	GL4r	0.03	-0.02
NOxF	GL3s	0.11	-0.10
NOxF	GL3r	0.08	-0.01
NOxF	GL4s	0.08	0.08
VOCF	GL3s	0.30	-0.30
VOCF	GL3r	0.17	0.11
VOCF	GL4s	0.09	-0.08

---

1 <sup>a</sup> TR2 = trapezoidal rule, 2 points. GL<sub>n</sub><sub>x</sub> = Gauss-Legendre formula using *n* points and *x* as the  
2 integration variable.

3 <sup>b</sup> Hourly average over the 3-day simulation.

4

## 1 **Figure captions**

2 Figure 1. Three possible integration paths when the concentration difference between the base  
3 (point B) and background (point b) cases is allocated to two sources with emissions scaled by  
4  $\lambda_1$  and  $\lambda_2$ . Path 1: equal control of emissions from both sources (diagonal path). Path 2:  
5 emphasis on control of emissions from source 1 first followed by control of emissions from  
6 source 2. Path 3: opposite of Path 2. Points b1 and b2 have the emissions from the background  
7 case plus source 1 and source 2, respectively.

8 Figure 2. Results from the 2-cell model simulations. Ozone and formaldehyde concentrations  
9 for the base case and the background case and the difference between them (anthropogenic  
10 increment).

11 Figure 3. Dependence of the integrands for allocating  $O_3$  to sources on the distance  $s$  along the  
12 Diag, NOxF and VO CF paths. The integrand (Eq. (4)) is calculated at the time of peak  $O_3$  on  
13 day 3 (66 h).

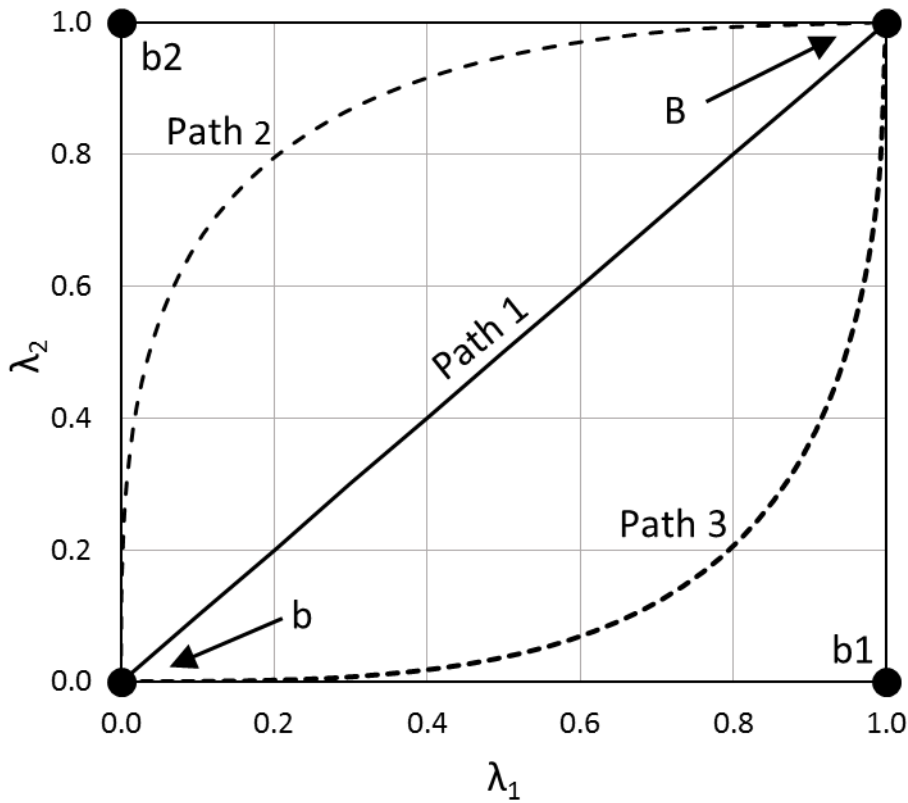
14 Figure 4. Contributions of sources and VOC,  $NO_x$ , CO, and HONO emissions to the  
15 anthropogenic  $O_3$  increment. Results are for the Diag path.

16 Figure 5. Apportionment of the anthropogenic  $O_3$  increment (left) and the FORM increment  
17 (right) to sources using the Diag, NOxF, and VO CF emission-control paths.

18



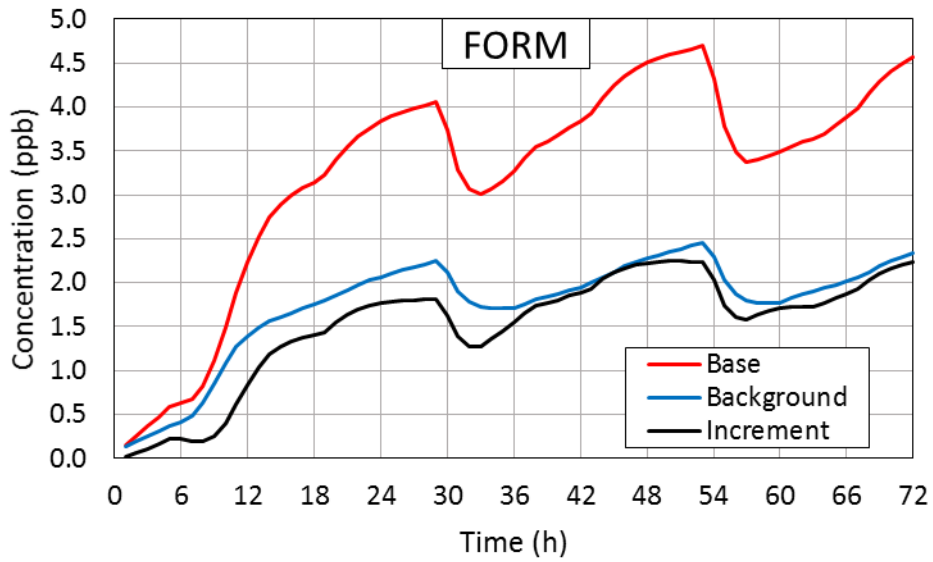
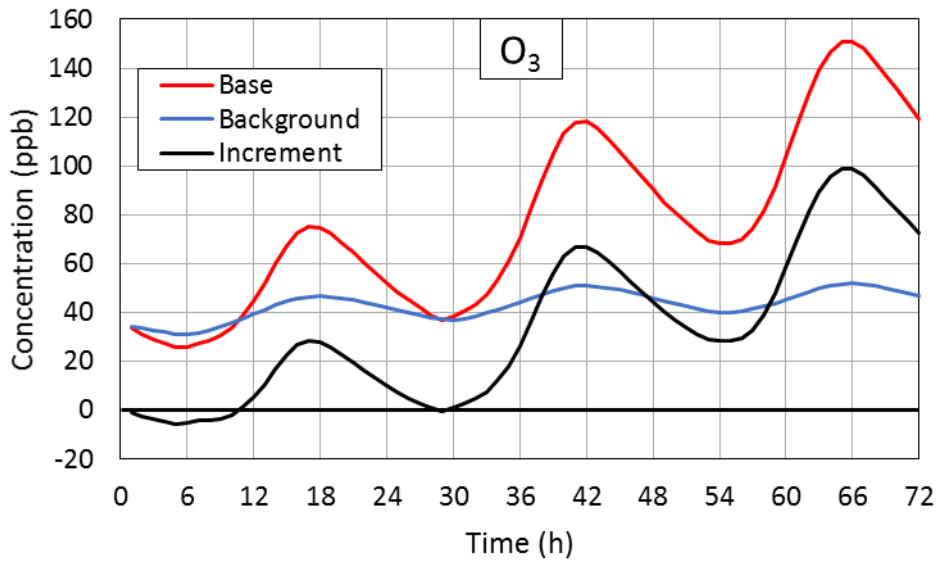
1



2

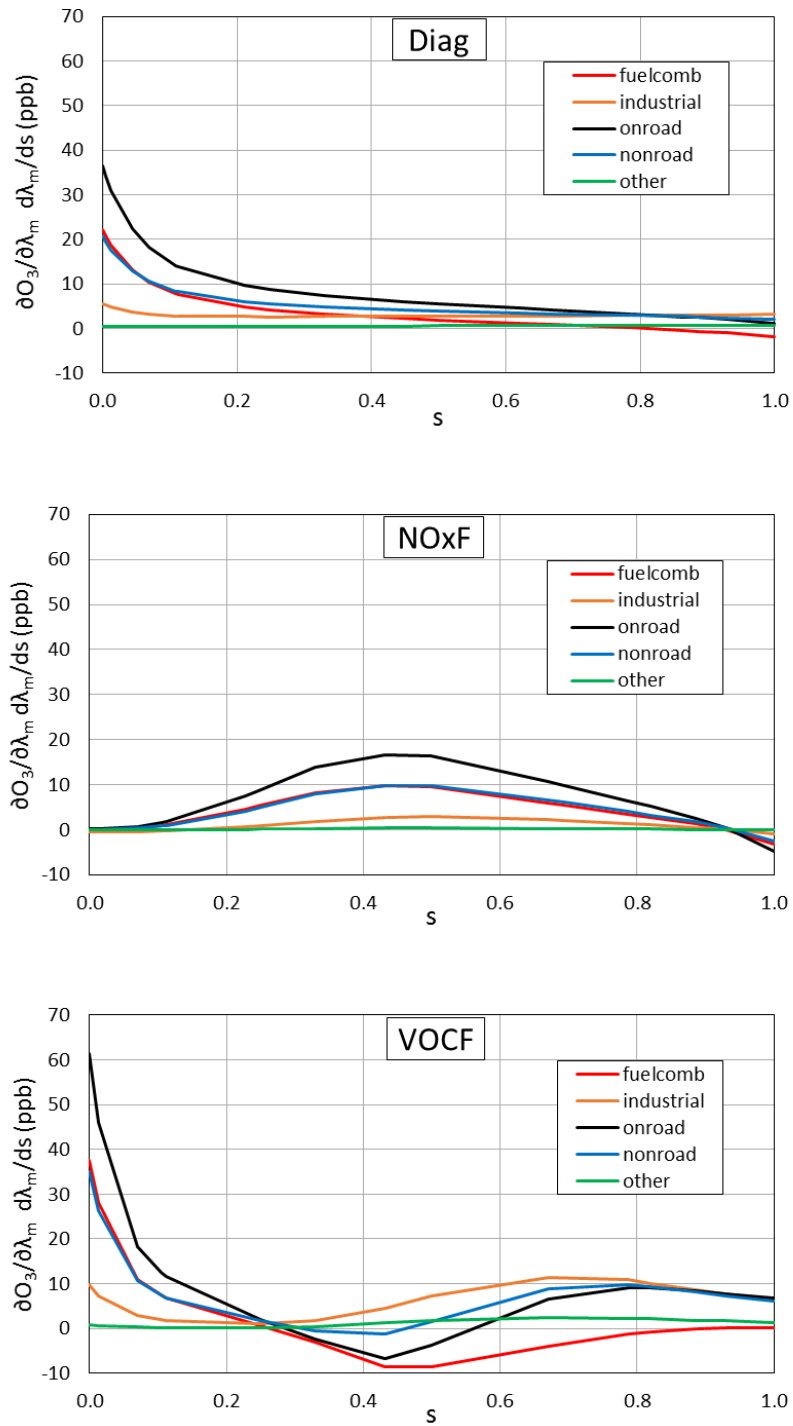
3 Figure 1. Three possible integration paths when the concentration difference between the base  
4 (point B) and background (point b) cases is allocated to two sources with emissions scaled by  
5  $\lambda_1$  and  $\lambda_2$ . Path 1: equal control of emissions from both sources (diagonal path). Path 2:  
6 emphasis on control of emissions from source 1 first followed by control of emissions from  
7 source 2. Path 3: opposite of Path 2. Points b1 and b2 have the emissions from the background  
8 case plus source 1 and source 2, respectively.

9



1  
2  
3  
4  
5

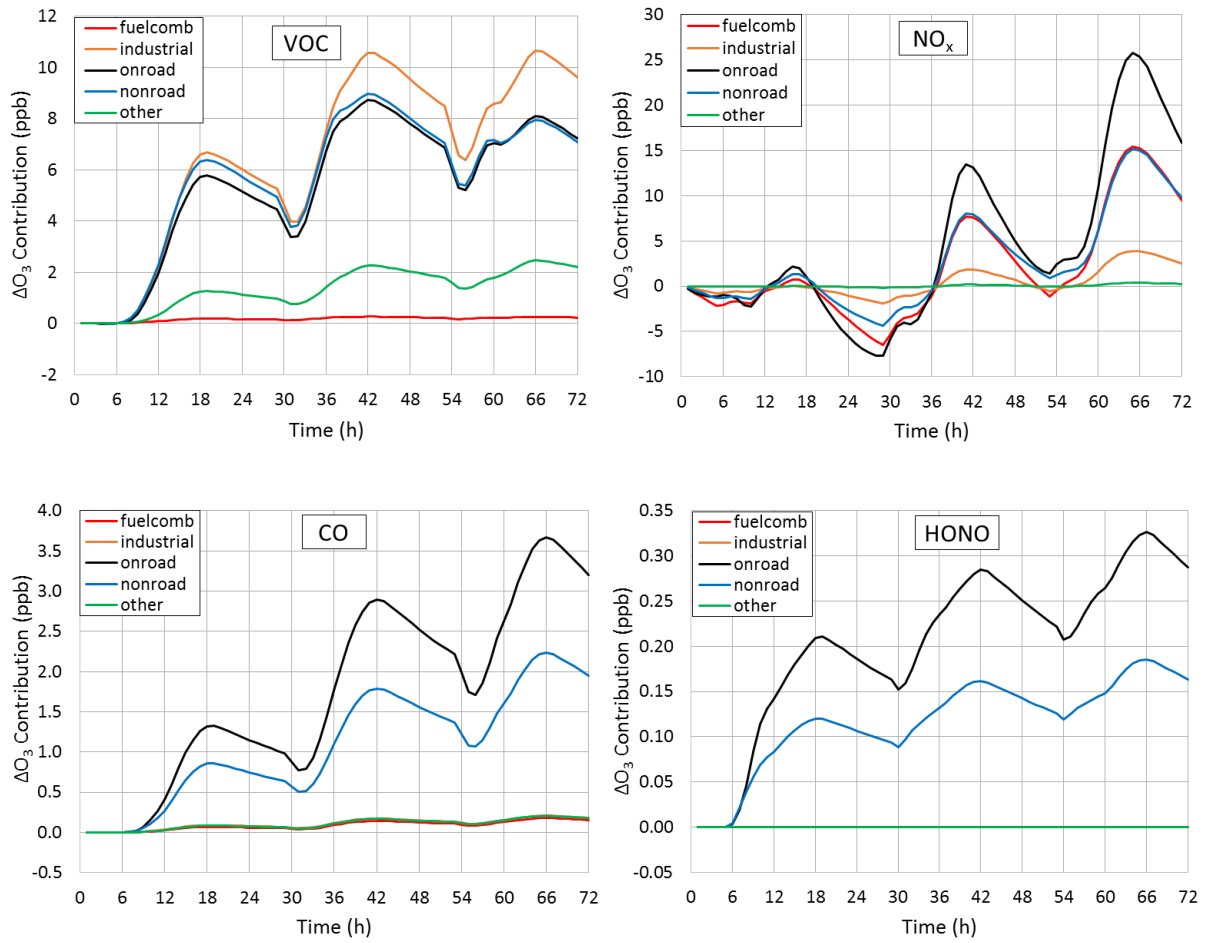
Figure 2. Results from the 2-cell model simulations. Ozone and formaldehyde concentrations for the base case and the background case and the difference between them (anthropogenic increment).



1

2 Figure 3. Dependence of the integrands for allocating  $O_3$  to sources on the distance  $s$  along the  
 3 Diag, NOx and VOx paths. The integrand (Eq. (4)) is calculated at the time of peak  $O_3$  on  
 4 day 3 (66 h).

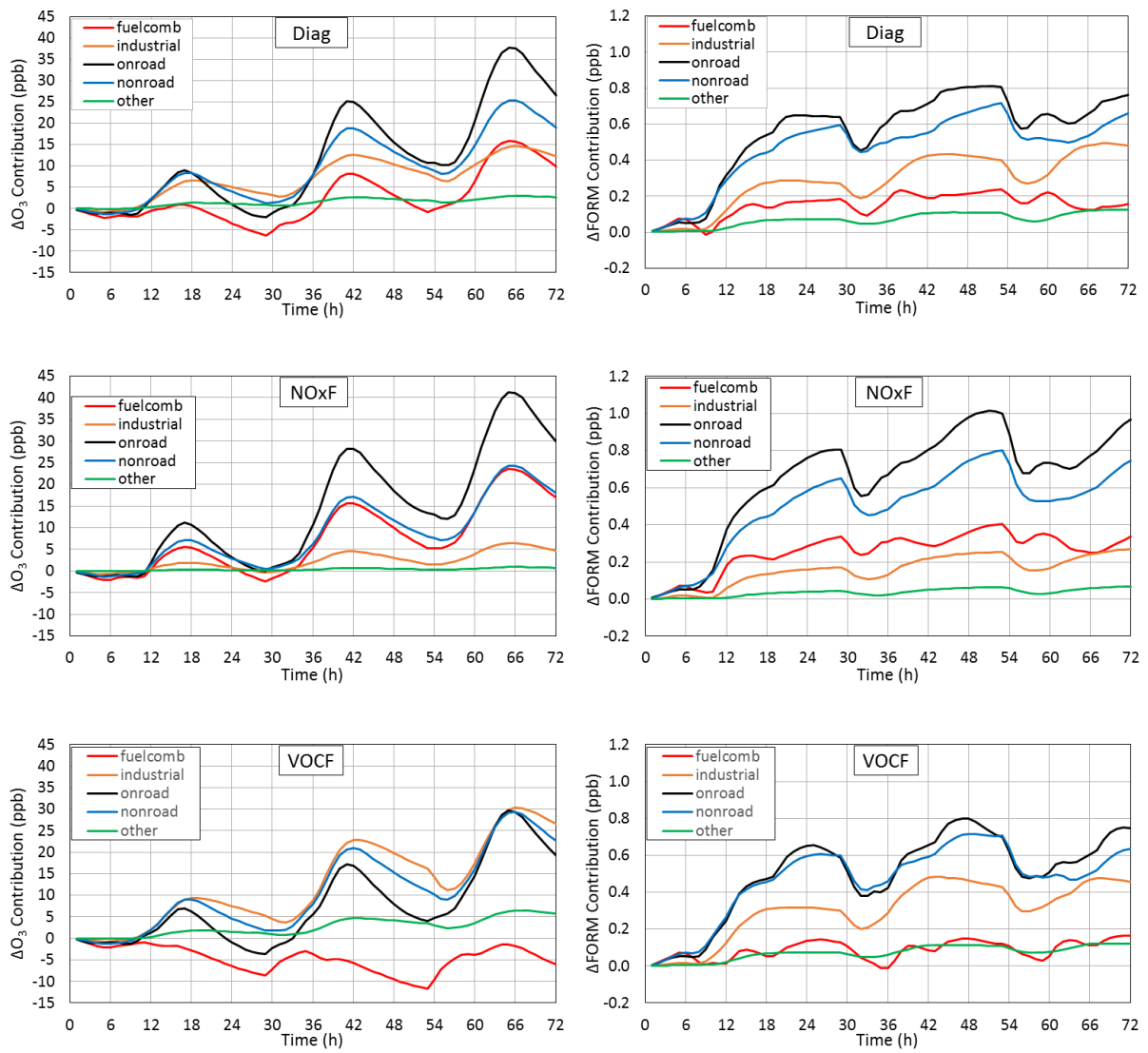
5



1

2 Figure 4. Contributions of sources and VOC,  $NO_x$ , CO, and HONO emissions to the  
 3 anthropogenic  $O_3$  increment. Results are for the Diag path.

4



1

2 Figure 5. Apportionment of the anthropogenic  $O_3$  increment (left) and the FORM increment  
 3 (right) to sources using the Diag, NOxF, and VOCF emission-control paths.